IET Image Processing

Special Section: Multidisciplinary advancement of imaging technologies: from medical diagnostics and genomics to cognitive machine vision, and artificial intelligence

IET Journals
The Institution of Engineering and Technology

Automatic grading of brain tumours using LSTM neural networks on magnetic resonance spectroscopy signals

ISSN 1751-9659
Received on 27th October 2019
Revised 4th December 2019
Accepted on 27th January 2020
E-First on 18th June 2020
doi: 10.1049/iet-ipr.2019.1416
www.ietdl.org

Emre Dandil[1] ✉, *Ali Biçer*[1]

[1]*Department of Computer Engineering, Bilecik Seyh Edebali University, Gulumbe Campus, Bilecik, Turkey*
✉ *E-mail: emre.dandil@bilecik.edu.tr*

Abstract: Brain tumours have increased rapidly in recent years as in other tumour types. Therefore, early and accurate diagnosis of brain tumour is vital for treatment. Magnetic resonance imaging (MRI) and histopathological assessments are the most common methods used in the detection of brain tumours. The research studies on non-invasive imaging methods such as MRI and magnetic resonance spectroscopy (MRS) have become widespread in recent years for brain tumour detection. In this study, a computer-assisted method is proposed for automatic grading of brain tumours on MRS signals. The classification of brain tumours with different grades is performed using long short term memory (LSTM) neural networks. In addition, additional features from MRS signals based on spectral entropy and instantaneous frequency are extracted. As a result of the experimental studies on the international MRS database (INTERPRET), it is seen that grading is achieved using the proposed method with average accuracy of 98.20%, sensitivity of 100%, and specificity of 97.53% performance results in three test studies carried out for the classification of brain tumour. Furthermore, in the grading of brain tumours using the proposed method, the average area under of the receiver operating characteristic curve is measured with high performance of 0.9936.

1 Introduction

Malignant tumours (cancers) are one of the most fatal diseases in the world. The highest death rate is referred to as cancer types after cardiovascular diseases on a global level [1]. Accurate diagnosis and treatment plan of tumours is of vital importance depending on their location. According to the estimates of the International Agency for Research on Cancer, if cancer incidences indicate a similar trend, 24 million new cases in 2030 and 29 million new cases in 2040 are expected to occur [2].

Brain tumours, as other tumour types, have a great risk for life. Some brain tumours are non-cancerous and known as benign, and some brain tumours are cancerous and defined as malignant [3]. According to the Global Cancer Statistics Report published in 2018, central nervous system tumours, especially the brain tumours, are the 19th most common tumour type in the world, and ~297,000 people die of this disease and 241,000 new patients are diagnosed every year. It is also stated in the same report that the central nervous system is the first leading cause of the deaths among cancer-related deaths. In addition, 4–8 new cancer incidences per 100 thousand are seen in developed and developing countries. On the other hand, this incidence doubles in under-developed and multi-ethnic countries. Although the incidence of brain tumours according to age distribution is highest in children, adults between the ages of 45–70 are in the second rank in terms of incidence of the brain tumours. World Health Organisation (WHO) divides into grades of brain tumours (central nervous system tumours) such as grade I (GI), grade II (GII), grade III (GII), and grade IV (GIV) [4]. Glioblastomas (WHO GIV malignant a type of brain tumour) are seen in men in a widespread manner, while benign meningioma's (MEN's; WHO GI benign a type of brain tumour) are significantly more common in women [5].

The number of people who have brain tumours and deaths from this disease continues to increase every year. Primarily, the type and grade of the brain tumour should be determined accurately for the planning of the treatment. Early diagnosis and detection of brain tumour have a significant value in terms of survival of patients. Magnetic resonance imaging (MRI), biopsy, and pathological findings are often used to help diagnose brain tumours. Brain imaging techniques allow doctors and researchers to view the activity or problems regarding the human brain without invasive neurosurgery. There are many imaging methods that use to examine the brain without having to do surgery [6]. Imaging methods such as computed tomography, positron emission tomography, and MRI can provide information about brain tissues from various excitation sequences. MRI is one of the imaging methods used commonly in the evaluation of brain tumours. In the brain MRI, the tumour may appear clearly and this situation can need the quantification of the tumour area in the treatment process for physicians [7]. MRI also provides superior contrast for different brain tissues when compared to all other imaging methods. In the meanwhile, MRI is efficient in the detection and identification of the brain tumours since it provides high contrast of soft tissues with high spatial resolution. It is a non-invasive technique and does not produce any harmful radiation [8].

Histopathological evaluation known as biopsy is the most accurate method for the detection of tumours [9]. However, a 1.7% mortality rate has been reported with biopsy procedures [10]. In addition, it is very difficult to determine the type and grade of the tumour using MRI [11]. The pathological examination of the brain causes great risks since it requires an operational process due to its location and function [12, 13]. In addition to MRI, the use of magnetic resonance spectroscopy (MRS) in the diagnosis of the brain has increased significantly in recent years, and various studies have been conducted on MRS. The metabolite level of the human brain can be measured using proton MRS (^{1}H MRS) in a non-invasive manner [14]. MRS imaging is also a quantitative method used to measure brain concentrations, chemicals, or brain metabolites using the MRI scanners [15]. Clinical and pattern recognition-based classification of brain tumours using MRS data has been thoroughly investigated for a long time [12, 16–24].

Grading of brain tumours is important for the determination of conformable treatment plan, following-up the disease and evaluation of prognosis. Treatment procedures such as tumour resection, radiation, and chemotherapy are generally performed for high-grade gliomas, while in low-grade gliomas, surgical treatment or tumour resection is realised mostly [25]. Although the gold standard for tumour grading is still histopathological evaluation, it has some limitations such as sampling error [26]. Therefore, in addition to advanced MRI techniques for staging brain tumours,

non-invasive diagnostic tools on MRS can provide more information within brain tumour grade. Recent studies relating to MRS express that it is a robust imaging method for grading and progression of brain tumours because of associating with metabolic changes [27, 28].

The rest of the paper is organised as follows. Section 2 provides a comprehensive literature survey. Section 3 describes ^{1}H-MRS. Section 4 explains the methods and materials used in the proposed approach. The proposed methodology is presented in Section 5. Section 6 analyses the experimental results and the discussions on the proposed work are in Section 7. Finally, Section 8 concludes the study with the obtained results and explains the future works.

2 Related works

The computer-assisted clinical decision-support systems on MRS have been studied intensively in the diagnosis of the brain tumours. In a multi-national study [24], the MRS imaging method provided high accuracy (ACC) in the diagnosis of the paediatric brain tumours and it is suggested that this method can become part of routine clinical assessment. According to a study conducted at Larissa University Hospital [23], MRS and computer-based decision support systems provided more successful results in distinguishing benign and malignant tumours. In addition, MRS may improve the restriction of cancerous brain tissue for radiation therapy planning [29]. Moreover, it can help tumour localisation for stereotactic biopsy [30] and surgical resection [31].

There are many studies conducted on the diagnosis and classification of brain tumours using MRS [16, 18, 32–38]. In a study conducted on the International network for pattern recognition of tumours using magnetic resonance (INTERPRET) dataset, Bayesian neural networks were used in the diagnosis of the brain tumours using the MRS data and accurate classification was provided within the study [39]. Naser *et al.* [40] investigated the usefulness of MRS in the grading of primary brain tumours. Manias *et al.* [41] aimed to assess the paediatric brain lesions using ^{1}H-MRS since MRS resulted in improved ACC and confidence in non-invasive diagnosis of paediatric brain lesions. However, it was not successfully used in clinical applications. Zeng *et al.* [11] suggested the non-invasive evaluation of grading of cerebral glioma using multi-voxel 3D ^{1}H MRS. Zou *et al.* [42] used the combination of multi-voxel ^{1}H MRS and diffusion tensor imaging in the classification of glioma brain tumours.

Recently, deep neural network-based methods such as convolutional neural network (CNN), long short term memory (LSTM) have been widely preferred in the processing of medical signal and images [43]. Especially, tumour segmentation, detection, recognition, and classification are among the most commonly applied processes on data. However, fewer studies have been proposed regarding tumour grading compared to these procedures. In this way, many brain tumour grading systems have been implemented on clinical decision support systems in recent years. Although there are many studies on the grading of brain tumours in the literature, it is seen that most of them are proposed on MRI images. There are fewer studies on the grading and detection of brain tumours using MRS. Of course, the difficulty of collecting and processing MRS data plays a significant role in this. In the grading of brain tumours, decision support systems, classification and clustering-based methods and machine learning-based methods are commonly used, as well as statistical methods that are widely used in clinical studies and evaluating the change of MRS metabolites. Table 1 summarises as comparative the studies proposed in the literature on the staging of a brain tumour on both MRS signals and MRI images.

When the previous studies are examined, it is seen that the studies on detection and grading of brain tumours on MRS signals are generally used as a supportive method, besides MRI and histopathological assessment methods. In this study, a deep learning-based LSTM neural network model is proposed to classify brain tumour grades according to WHO standards. For the robust analysis of MRS signals, additional features from MRS signals are extracted using spectral entropy and instantaneous frequency. Next, the extracted features within MRS signals are augmented using augmentation techniques. Finally, the brain tumour is classified into four grades such as GI, GII, GIII, and GIV using a deep LSTM model. Thus, the proposed model can be used as a second tool for the decision-making of radiologists and physicians and give some recommendations for tumour grading for clinical examinations. The important contributions of the proposed study can be explained as follows:

(i) this study is the implementation of a computer-aided diagnosis/detection system for a grade classification of a brain tumour within WHO standards,
(ii) accurate grading of brain tumours on MRS signals is achieved using LSTM neural networks without the need for other tumour detection systems,
(iii) this study is one of the few recent studies proposed both on MRS and based on LSTM deep learning method,
(iv) the proposed LSTM model has achieved higher ACC for brain tumour grading on brain MRI images and MRS signals compared to other state-of-the-art methods summarised in Table 1.

3 Magnetic resonance spectroscopy (MRS)

Although MRI is the most widely used imaging method for the detection of brain tumours, it has some limitations. The obtained magnetic resonance (MR) images are examined and evaluated by the physicians. However, in some cases, it is not possible for physicians to assess the data on the available MR images and decision making for diagnosis because this decision can lead to irreversible consequences for patients. Therefore, various MRI techniques have been developed to prevent these conditions to assist physicians and to provide a more accurate diagnosis. Detection and grading of brain tumours with MRS is one of these methods as well [21].

MRS is a kind of MR scanning and its implementation method is generally not different from MR. MRS, which is implemented in an MR tool with high Tesla value, is one of the tools used to determine the molecular structure of the compounds and to detect the presence of the compound. There are two types of MRS imaging methods such as single-voxel and multi-voxel [51]. Since MRS is a method of examining the chemical structure of the brain, some atomic nucleus is used during these measurements. ^{1}H (proton) atom is the most widely used atomic nuclei and it can provide precise measurements. In addition, the ^{23}Na (sodium) and ^{31}P (phosphorus) atoms are also used during the MRS process [52]. The MRS process can be performed within 10–15 min. Since the MRS method is a process that examines the chemical structure of the brain, it is used in the diagnosis of brain tumours as well as a strike to the head, epilepsy, metabolic disorders, infections, and psychological diseases. A sample of MRS signal patterns obtained from a healthy individual is shown in Fig. 1.

MR images obtained in a 22-year-old male with biopsy verified GIV glioblastoma brain tumour and MRS spectrum signals obtained from normal brain tissue (NOR) and tissues with masses are shown in Fig. 2. As can be seen in the axial plane of a T2-weighted MR image presented in Fig. 2*a*, there is a mass in the left frontal lobe. The ^{1}H MRS signals of the voxel obtained from the normal tissue of the brain and the MRS signals of the mass obtained from the tumour region of the brain are presented in Figs. 2*b* and *c*, respectively. An extreme decrease is observed in *N*-acetyl aspartate (NAA) peak at 2.02 ppm and an increase is observed in choline (Cho) peak at 3.22 ppm. In addition, an excessive reverse change is seen clearly at the lactate (Lac) peak, which has a double peak at 1.33 ppm. These findings are very strong indicators of glioblastoma, which is the WHO GIV brain tumour. The ratio of some metabolites in the spectrum also provides information about the type and grade of the tumour. When the spectrum of glioblastoma brain tumour lesion in Fig. 2*b* is examined, according to the spectrum of NOR presented in Fig. 2*a*, the findings of an increase in Cho/creatine (Cre) ratio, an increase in Cho/NAA ratio, and an increase in Lac/Cre ratio are the strong indicators of glioblastoma. These findings are strong inferences

Table 1 Comprehensive comparative overview of the existing studies for brain tumour grading with key differences

Paper and year	Dataset	Data type	Number of data	Method	Tumour and grade type	Performance results	Evaluations
Law *et al.* [37], 2003	their own dataset	T_2-weighted perfusion MR, MRS	160	statistical analysis methods	low-grade and high-grade glioma	SEN, SPE, positive predictive value, and negative predictive value of 95.0%, 57.5%, 87.0%, and 79.3%, respectively	• there is no machine learning method based on classification • only statistical methods were used • in the evaluation of MRS data, ratios such as Cho/Cre, Cho/NAA, and NAA/cr were measured only
Tate *et al.* [18], 2006	INTERPRET database [44]	in vivo single voxel MRS	241	DSS – a tool for classification	low-grade (GI–GII) and high-grade glioma (GIII–GIV), MEN, metastasis	89.0% ACC for test sets, including 91 cases	• no feature extraction from MRS data. • DSS for brain tumour diagnosis with MRS showed a small improvement over MRI used alone
Weis *et al.* [34], 2010	their own dataset	single voxel MRS	20	statistical analysis (mean and standard deviation)	low-grade and high-grade glioma	standard deviation and mean values of concentrations of metabolites were compared	• only statistical methods were used • the number of MRS data is few • there is no machine learning method based on the classification
Chen *et al.* [45], 2011	their own dataset	high-resolution magic-angle spinning nuclear MRS	30	principal component analysis (PCA), SIMCA (a soft independent modelling of class analogy), statistical analysis	astrocytoma (GI), astrocytoma (GII), anaplastic astrocytoma (GIII), glioblastoma (GIV), and medulloblastoma (GIV)	ACC of 87%, SEN of 87% and SPE of 93%	• the number of MRS data is few • no feature extraction from MRS data • real values of concentrations of metabolites were used for distinguishing
Server *et al.* [26], 2011	their own dataset	MRS imaging	74	statistical analysis methods	low-grade and high-grade glioma	Cho/Cre and Cho/NAA metabolite ratios resulted in SEN, SPE, positive predictive value, and negative predictive value of 91.5%, 100%, 100 and 60% respectively	• no feature extraction from MRS data • real values of concentrations of metabolites and some ratios were used for grading • there is no machine learning method based on the classification
Zeng *et al.* [11], 2011	their own dataset	multi-voxel 3D MRS	39	statistical analysis methods and metabolite peak ratios	low-grade and high-grade glioma	SEN, SPE, positive predictive value, and negative predictive of 84.00%, 83.33%, 91.30% and 71.43%, respectively.	• no feature extraction from MRS data. • real values of concentrations of metabolites and some ratios were used for grading • there is no machine learning method based on classification

Paper and year	Dataset	Data type	Number of data	Method	Tumour and grade type	Performance results	Evaluations
Zou *et al.* [42], 2011	their own dataset	MRI, diffusion tensor imaging, multi voxel MRS	30	statistical analysis methods and metabolite peak ratios	low-grade and high-grade glioma	kappa value = 0.798	• the number of MRS data is few. • no feature extraction from MRS data. • real values of concentrations of metabolites and some ratios were used for grading • there is no machine learning method based on classification
Julià-Sapé *et al.* [46], 2012	INTERPRET database [44]	in vivo single voxel MRS, MRI	40	DSS software (DSS, jMRUI, DMS) developed by GABRMN	astrocytoma (GI), astrocytoma (GII), anaplastic astrocytoma (GIII), glioblastoma (GIV), medulloblastoma (GIV), metastasis, abscess, MEN, melanocytoma, adenoma, multiple sclerosis, lymphoma	AUC = 0.93	• a comprehensive MRS database • some DSS software such as DSS, DMS, jMRUI • many test procedures • there is no machine learning method based on classification
Wang *et al.* [47], 2015	their own dataset	in vivo multi-voxel MRS	259	Linear discriminant analysis (LDA) and least squares-support vector machine (LS-SVM)	low-grade (GI–GII) and high-grade glioma (GIII–GIV), metastasis, normal tissue	• 87.7% ACC for grading • 95.0% ACC for classification NOR and tumour	• no feature extraction from MRS data • peak values of metabolites such as Lip, NAA, Cho and Lac were used as features in classification
Anaraki *et al.* [48], 2019	Information eXtraction from Images Dataset (IXI), the Repository of Molecular Brain Neoplasia Data (REMBRANDT), the cancer genome atlas low grade glioma radiology data (TCGA-LGG), and their own dataset	MRI	1089 (total of all datasets)	CNN and genetic algorithm (GA)	low-grade and high-grade glioma, MEN, pituitary brain tumour	94.2% ACC	• grading was performed only using MRI data without MRS data
Sajjad *et al.* [49], 2019	radiopedia, and another brain tumour dataset [50]	MRI	3185 (total of two datasets)	CNN	low-grade and high-grade glioma, MEN	88.41%, 96.12%, and 94.58% for SEN, SPE, and ACC, respectively	• grading was performed only using MRI data without MRS data

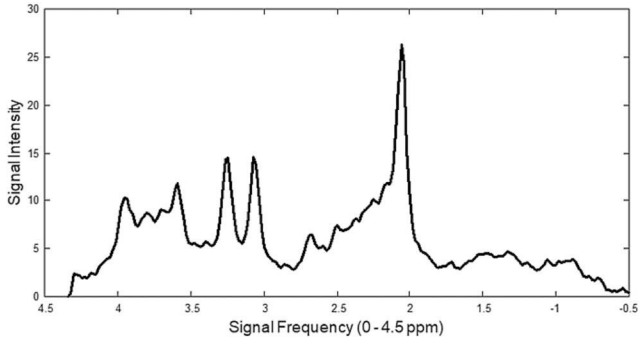

Fig. 1 *Sample of MRS signal pattern of the brain obtained from a healthy individual*

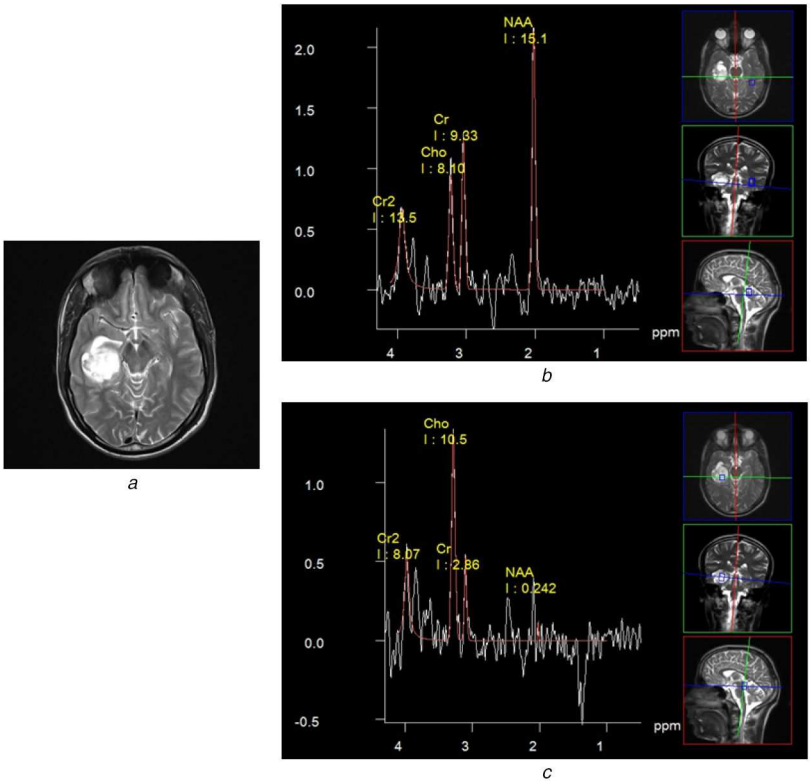

Fig. 2 *MR images obtained from a 22-year-old male with biopsy-verified a glioblastoma GIV brain tumour and MRS spectrum signals*

(*a*) Mass is seen in the left frontal lobe of the axial T2-weighted MR image, **(*b*)** ^{1}H MRS signals of the voxel taken from the normal tissue of the brain, **(*c*)** MRS signals of the mass taken from the tumour region of the brain

Table 2 Resonance ppm values and properties of some principal metabolites observed in MRS

Metabolite abbreviation	Resonance, ppm	Fundamental properties of the metabolite
Lip	0.9–1.33	disintegration of brain tissue
Lac	1.33	anaerobic glucose marker
NAA	2.0	symptoms of neuron health
Glx	2.0–2.46	stimulating neurotransmitter
	3.6–3.8	
Cho	3.2	cell metabolism, cell proliferation
Cre	3.03	cellular energy determinant
mI	3.55	osmolytic marker, recommended glial marker

that this is a high-grade glioma in which the case is deduced on the MRS signal.

MRS provides metabolic information about the brain. The principal brain metabolites detected during the MRS process are Cho, Cre, NAA, Lac, myo-inositol (mI), glutamine–glutamate (Glx), and lipids (Lip) [53, 54]. The resonance values of the metabolites observed in brain tumours in MRS and the properties of these metabolites are denoted in Table 2. In addition, the ratio of metabolites such as Cho/NAA, Cho/Cre, and NAA/Cre provides information about the presence of tumour [54].

4 Material and methods

4.1 MRS dataset

The data used in the study were prepared from the INTERPRET database [44]. The INTERPRET project is a multi-centre project and the data are collected from six different centres such as the Center Diagno'stics Pedralbes (CDP, Barcelona, Spain), St. George's Hospital Medical School (SGHMS, London, UK), Fundacíon para la Lucha contra las Enfermedades Neuroĺogicas de la Infancia (FLENI, Buenos Aires, Argentina), Institut de Diagno'stic per la Imatge (IDI, Barcelona, Spain), University Medical Center Nijmegen (UMCN, Nijmegen, The Netherlands) and Uniwersytet Medyczny w Lodzi (MUL, Lodzi, Poland). Scanning of the patients was performed with Siemens, General Electric, and Philips scanners. MRS signal data were obtained between 1994 and 2001 in the database. The infrastructure of the project includes MRS signals of glioblastoma multiforme (GBM), MEN, metastasis, diffuse astrocytoma, anaplastic astrocytoma, NOR, schwannoma, medulloblastoma, oligoastrocytoma, pilocytic astrocytoma (PAST), ependymoma, lymphoma, germinoma, hemangioblastoma, fibrosarcoma, abscess, and chordoma grades. The obtained ^{1}H-MRS data for GBM-GIV, MEN-GI, PAST GI, diffuse astrocytoma GII (DAST), anaplastic astrocytoma GIII (AAST), and NOR used in this study are presented in Table 3.

INTERPRET is a European Union-funded project carried out to facilitate the use of MRS for the diagnosis and treatment of patients with brain tumours. The main objectives of the project were to enable radiologists to classify brain tumours using MRS, to facilitate the use of MRS by clinicians, and to make MRS a viable alternative for brain biopsy. As a result of this project, a decision support system (DSS) developed for brain tumours, a fully operational database management system, and a descriptive database were developed. For this study, a dataset was created on MRS data obtained from the INTERPRET database, including 87 cases GBM GIV, 57 cases MEN GI, 22 cases DAST GII, three cases PAST GI, and ten cases AAST GIII. The distribution of the data used in this study is shown in Fig. 3.

The MRS data of each patient used in the study were aggregated within a dataset. MR images and MRS signals of a

Table 3 Number of cases for short time echo ^{1}H-MRS obtained from data centres within INTERPRET project

Data centre	Acquisition type	Number of cases						Total
		GBM	MEN	DAST	PAST	AAST	NOR	
CDP	STEAM	30	12	4	2	0	4	52
SGHMS	STEAM	12	4	6	0	4	5	31
	PRESS	6	8	4	0	3	7	28
FLENI	PRESS	2	0	1	0	0	0	3
IDI	PRESS	31	30	5	1	3	5	75
UMCN	STEAM	2	1	1	0	0	10	14
MUL	STEAM	4	2	1	0	0	0	7
total		87	57	22	3	10	31	210

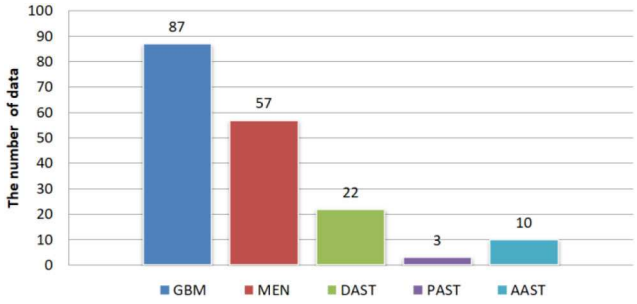

Fig. 3 *Distribution of MRS data used in the study*

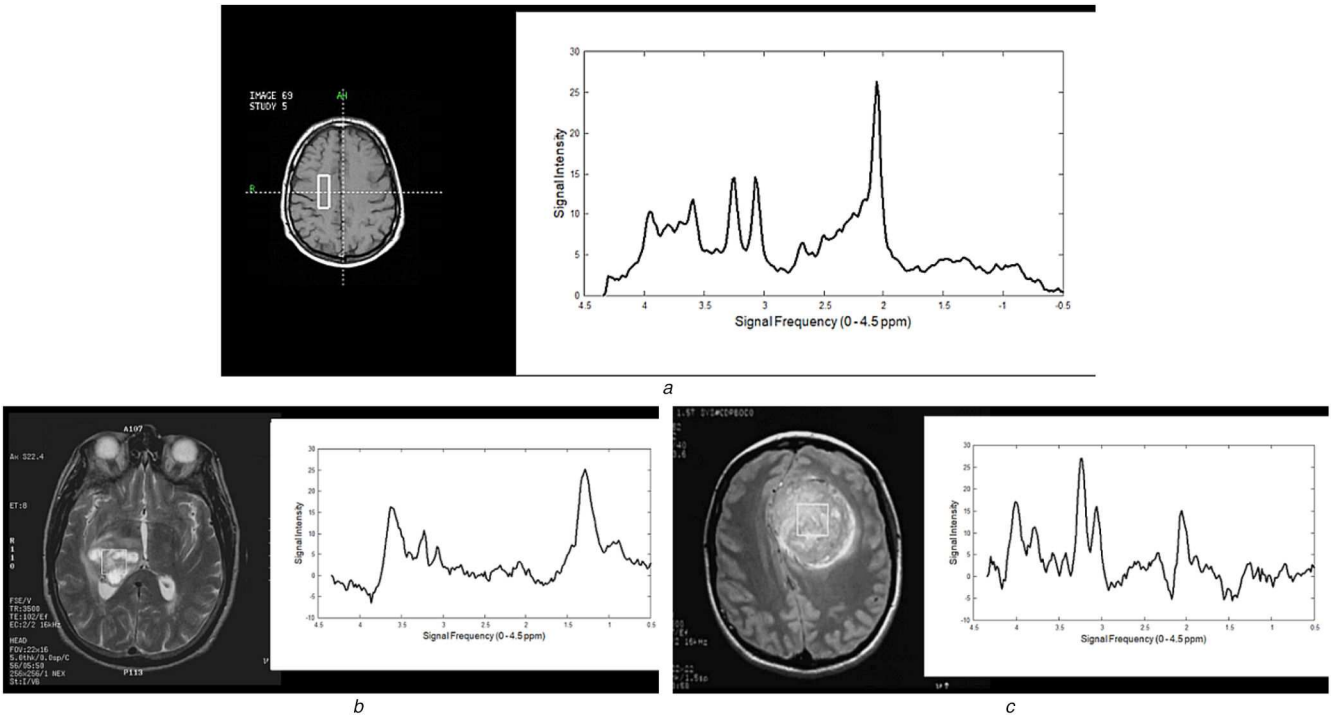

Fig. 4 *MRI images and MRS data for NOR and brain tumour samples*

(*a*) Axial anatomical plane MR image and MRS signal data of a patient with NOR, **(*b*)** Axial anatomical plane MR image and MRS signal data of a patient with GBM, **(*c*)** Axial anatomical plane MR image and MRS signal data of a patient with MEN

patient with NOR, MEN, and GBM obtained from the INTERPRET database are denoted in Figs. 4*a–c*, respectively.

4.2 LSTM neural networks

In this study, LSTM neural networks, a type of recurrent neural network (RNN), are used to train and test sets in the MRS database created for the classification and grading of brain tumours. The main reason for using LSTM is that the available MRS data is in the form of a vector and LSTMs are very successful in classifying the data in the form of vector. Although RNNs have been proven to be successful in array-priority tasks, it may be difficult to learn long-term dependencies, mainly due to the exploding/vanishing gradient problem caused by the gradient propagation of the recurrent network. LSTM networks can overcome this problem by incorporating memory units that allow the network to learn when to forget and update the previous memory states [55].

LSTM was proposed by Hochreiter and Schmidhuber and improved and popularised by Alex Graves recently [56]. LSTM has achieved considerable success on many issues and has been widely used. Some of these studies are LSTM-based traffic flow prediction, expression recognition, speech recognition, sentiment classification, wind power forecasting based on sequential correlation, financial time series forecasting model with missing data [57, 58]. LSTM is developed from the RNN architecture and it contains a processor, which determines whether the information is

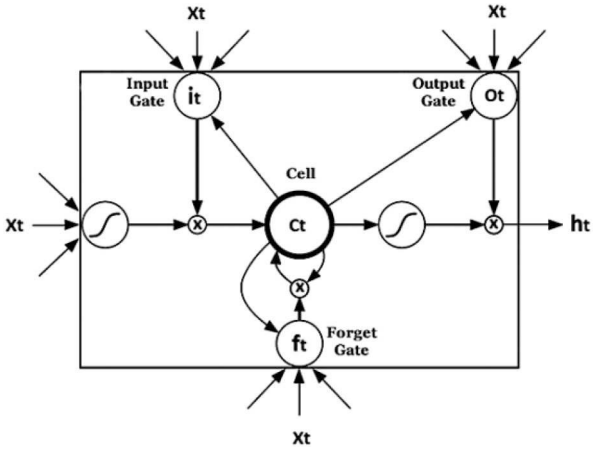

Fig. 5 *Cell structure of typical LSTM [60]*

useful, and the working part of it is named as a cell [59]. There are three gates in a cell. These are the input gate, forget gate, and output gate. Input gate and forget gate both work on the state of the cell. However, the role of the input gate is to selectively record the new information. On the other hand, the forget gate aims to selectively forget information and provides information about the cell states. The output gate acts on the hidden output information [56]. The structure of the conventional LSTM cell is shown in Fig. 5.

Typical LSTM cell is composed of input, forget, and output gates, and a cell is composed of an activation component and is shown in Fig. 5. These units receive activation signals from different sources and control the activation of the cell by the designed multipliers. The LSTM gates can prevent the rest of the network from modifying the contents of the memory cells for multiple time steps. LSTM networks preserve signals and propagate errors for much longer than ordinary RNNs. Therefore, LSTM networks can process data with complex and separated interdependencies and allow the data to excel in a range of sequence learning domains [55, 60, 61]. The input gate equation of LSTM is given as follows:

$$i_t = \sigma(\boldsymbol{W}x_i x_t + \boldsymbol{W}h_i h_{t-1} + \boldsymbol{W}c_i c_{t-1} + b_i) \quad (1)$$

where $\boldsymbol{W}x_i$ is the weight matrix from the input layer to the input gate, $\boldsymbol{W}h_i$ is the weight matrix from the hidden state to the input gate, $\boldsymbol{W}c_i$ is the weight matrix from the cell activation to the input gate and b_i is the bias of the input gate. The equation of the forget gate is given as follows [55, 60, 61]:

$$f_t = \sigma(\boldsymbol{W}x_f x_t + \boldsymbol{W}h_f h_{t-1} + \boldsymbol{W}c_f c_{t-1} + b_f) \quad (2)$$

where $\boldsymbol{W}x_f$ is the weight matrix from the input layer to the forget gate, $\boldsymbol{W}h_f$ is the weight matrix from hidden state to the forget gate, $\boldsymbol{W}c_f$ is the weight matrix from the cell activation to the forget gate and b_f is the bias of the forget gate. Cell state is given as follows [55, 60, 61]:

$$C_t = f_t c_{t-1} + i_t \tanh(Wx_c x_t + Wh_c h_{t-1} + b_c) \quad (3)$$

where $\boldsymbol{W}x_c$ is the weight matrix from the input layer to the cell gate, $\boldsymbol{W}h_c$ is the weight matrix from the hidden state to the cell gate, and b_c is the bias of the cell gate. The equation of the output gate is given in (4) [55, 60, 61]

$$o_t = \sigma(Wx_o x_t + Wh_o h_{t-1} + Wc_o c_t + b_o) \quad (4)$$

where $\boldsymbol{W}x_o$ is the weight matrix from the input layer to the output gate, $\boldsymbol{W}h_o$ is the weight matrix from the hidden state to the output gate, $\boldsymbol{W}c_o$ is the weight matrix from the cell activation to the output gate and b_o is the bias of the output gate. The equation given in (5) is defined as the hidden state [55, 60, 61]

$$h_t = o_t \tanh(c_t) \quad (5)$$

Finally, we need to decide what to send to the output. This output will be based on our cell state. First, the sigmoid layer is executed, which decides what parts of the cell state are output. Then, the cell state is put through the tanh layer in a way to push the values to be between −1 and 1 and multiplied by the output of the sigmoid gate. Therefore, it is ensured that only the parts that are decided are transferred to the output [61, 62]. In addition to the standard LSTM structure, there are other LSTM structures. In this study, a deep bi-directional LSTM (Bi-LSTM) structure was used. Bi-LSTM allows stacking hidden layers of LSTM cell in space. In addition, it increases the capacity of the RNN. Bi-LSTM networks are more powerful than unidirectional LSTM networks. These networks theoretically involve all information of input sequences during computation. Bi-LSTM is widely used for different applications such as language understanding due to its distributed representation feature. The Bi-LSTM model both utilises the same advantages discussed in the bi-directional RNN section, and overcomes the vanishing gradient problem [61].

5 Proposed methodology

The flowchart of the architecture proposed by the Bi-LSTM network used in this study is given in Fig. 6 for grading of brain tumours on MRS signals. The input data of the network are the property sequences of the MRS signals. LSTM networks can learn the long-term dependencies between time steps of sequence data. Therefore, feature extraction is performed by looking at both forward and backward data. Since each of the input signals has a size, the input size is indicated as one-dimensional arrays. After the initial training, the input sequences are re-arranged as bi-dimensional in order to obtain more successful results. A Bi-LSTM layer with an output size of 100 is determined and the output of the last element of the vector is obtained. The Bi-LSTM layer is then matched to 100 features with the time series output size, and then output is set for the fully connected layer. Finally, two classes are specified for the two-dimensional fully connected layer, which followed by the softmax layer and the classification layer.

5.1 Creating training/test sets and defining the LSTM network

In the first stage of the proposed LSTM model, the dataset is split into mini-batches for training and testing. Then, the function spreads or cuts the signals in the same mini-batches, so that the signals have the same length. On the other hand, too much spreading or cutting can adversely affect the performance of the network since the network may mis-interpret a signal based on added or removed data. The MRS signals generated in the previous section are used to design the classifier. To train the classifier, the

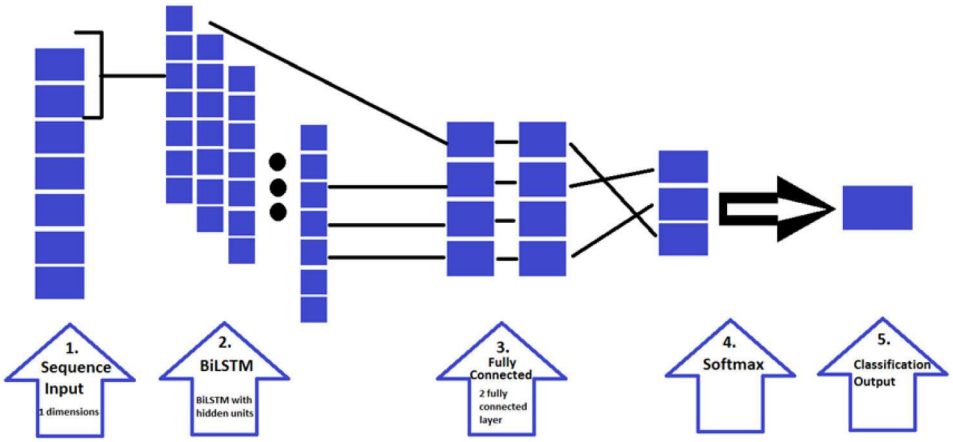

Fig. 6 *LSTM network architecture proposed in this study*

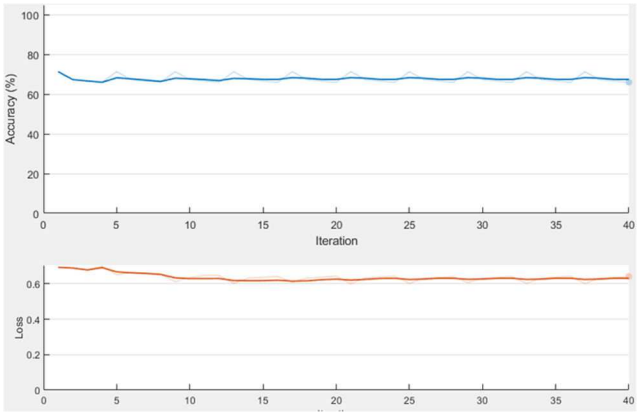

Fig. 7 *Training plot of the proposed LSTM network*

MRS signals are passed to a training set and a testing set to test the ACC of the classifier on the new data. When the number of signals is more than the other signal, the less data is duplicated since this situation can cause errors during the training process. This duplication, which is commonly referred to as sampling, is a form of data growth used in deep learning [63]. At this stage, the signals are split into two parts. The distribution between the MRS signals of the brain tumours is then evenly balanced in both the training set and the testing set.

LSTM networks can learn the long-term dependencies between the time steps of sequence data. In this study, the LSTM layer looks at the sequence in both the forward and backward directions. Since each of the input signals has a size, the input size is specified to be sequences of one size. A Bi-LSTM layer with an output size of 100 is created and the last element of the sequence is the output. Lastly, a fully connected softmax layer and a classification layer are added to the model as seen in Fig. 6.

5.2 Training of LSTM network

In this stage, training is provided on the data used for the training in the LSTM network. The top-subplot of the training-progress shows the training ACC, which is the classification ACC in each mini-batch. As the training progresses successfully, this value is generally expected to increase towards 100%. The training phase of the LSTM network is shown in Fig. 7. The bottom sub-plot shows the training loss, which is the cross-entropy loss in each mini-batch. When the training progresses successfully, this value is generally expected to decrease towards zero. However, it is generally observed that during training, the plots oscillate between values without a certain upward or downward trend. This oscillation means that the training sensitivity (SEN) has not improved and the loss of training has not decreased. This situation occurs at the start of the training or follows a horizontal trend. ACC in training can be improved after some preliminary improvement. In many cases, changing the training options can help the network achieve convergence. At the end of this process, it is reached that the success rate of the training varied between 60–70% as seen in Fig. 7. Since the training and test success at this stage varied between 60 and 70%, feature extraction and standardisation of the data are performed in order to increase the training success and test success.

5.3 Extracting additional features of MRS signals

The performance of the system is improved by extracting additional features from the MRS signals in order to help improve the training and test ACC of the LSTM classifier using spectrogram, instantaneous frequency, spectral entropy. Spectrograms showing the energy distributions of each signal type are extracted to decide which features are needed. For example, the spectrograms of MRS signals of MEN and glioblastoma type brain tumours are given in Fig. 8. As shown in this figure, the distribution of energy regions varies in both tumour types. In the next step, feature extractions for instantaneous frequency and spectral entropy are performed in the time plane according to these spectrogram data.

After the spectrograms are extracted, the first thing for extracting the spectral entropy is to obtain instantaneous frequencies from the MRS signals. The result of instantaneous frequency extraction for both signal types (MEN and GBM) in the time-frequency plane is presented in Fig. 9.

The spectral entropy measure how flat is the spectrum of a signal [64]. A signal with much spectrum and high oscillation has low spectral entropy. A signal with a flat spectrum, such as white noise, has high-spectral entropy. As with the instantaneous frequency estimation case, it uses time windows to calculate spectral entropy. The time outputs of the function correspond to the centre of the time window. The spectral entropy process is applied to the data in the application. Instantaneous frequency and spectral entropy process simplifies MRS data, which are very long and complicate by using the feature extraction method in time plane.

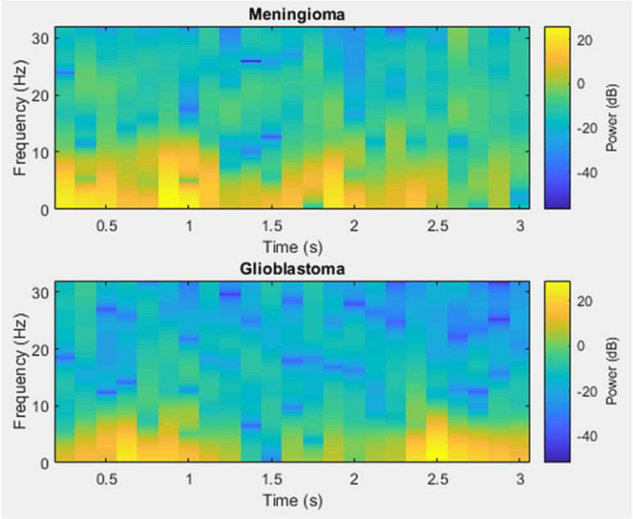

Fig. 8 *Spectrograms extraction from MRS signals*

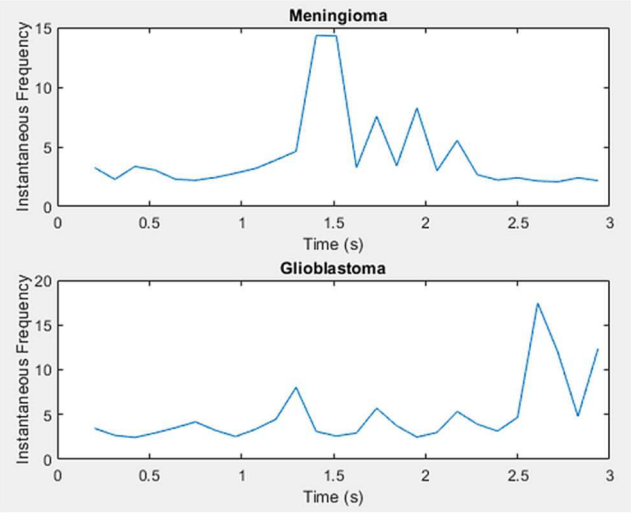

Fig. 9 *Instantaneous frequency extraction from MRS signals*

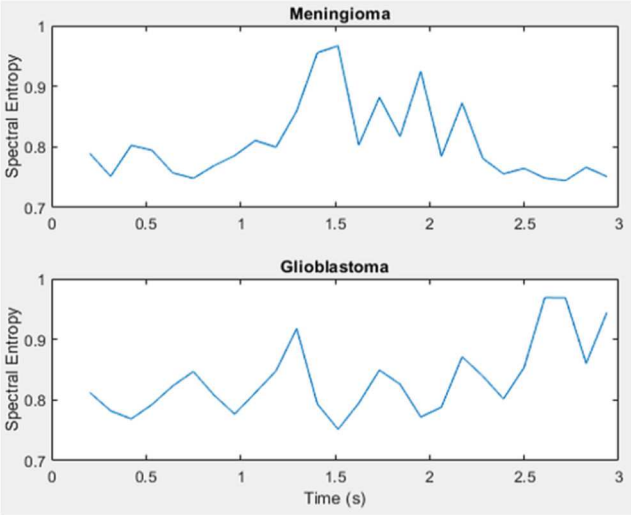

Fig. 10 *Representation of spectral entropy from MRS signals*

Therefore, training and testing time of the LSTM network is shortened and performance is improved. The representation of spectral entropy from MRS signals is denoted in Fig. 10.

The instantaneous frequency and spectral entropy have tools that differ by almost one order or magnitude. Furthermore, the mean of the instantaneous frequency might be too high for the LSTM to learn effectively. When a network has data with a large mean and a wide range of values, large inputs could slow down the learning and convergence of the network. The mean and standard deviation of the training set is calculated to standardise the training and test sets. Standardisation or standard deviation is used to improve network performance during training. Since each of the signals had two dimensions after the feature extraction and standardisation of data in the LSTM network, the input sequence size is also specified as two sizes and the network architecture is modified.

5.4 Re-training of the LSTM network

After the initial training and results, the signal data are re-arranged by feature extraction methods such as spectrogram extraction, instantaneous frequency extraction, spectral entropy, cell regulation, and data standardisation. After this process, MRS data are re-trained with the LSTM network on the application. The re-trained LSTM network is shown in Fig. 11. As a result of the retraining of the network, the performance plot of the training of the MRS signals approached towards 100% by showing oscillations and the loss plot decreased to 0%.

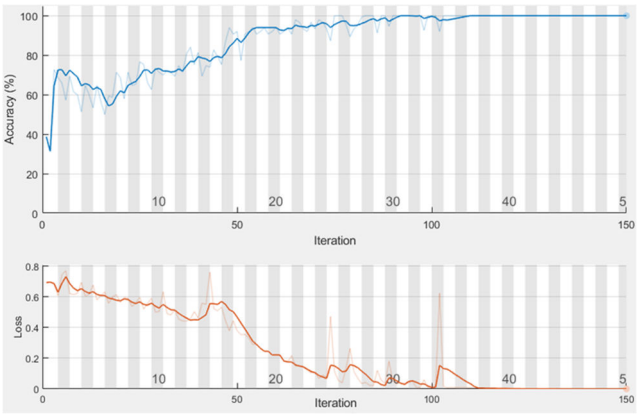

Fig. 11 *Re-training the LSTM network with time frequency data*

6 Experimental results

In this study, for the experimental studies, the MRS data of the brain tumours of GBM (87 MRS signal patterns), MEN (57 MRS signal patterns), PAST (three MRS signal patterns), DAST (22 MRS signal patterns) and AAST (ten MRS signal patterns) were used and the grading of brain tumours was provided. All experimental studies were carried out on a computer with 2.4 GHz i7 processor, 8 GB RAM, and NVIDIA GeForce GTX 1050 GPU using MATLAB programme and performance tests were performed.

Table 4 Distribution of the training and test data in MRS dataset

Test type	Number Of data	Training set (70%)	Test set (30%)
test 1: MEN versus GBM	432 × 200	302 × 200 (GBM = 183, MEN = 119)	130 × 200 (GBM = 78, MEN = 52)
test 2: PAST + DAST versus GBM	336 × 200	236 × 200 (GBM = 183, PAST + DAST = 53)	100 × 200 (GBM = 78, PAST + DAST = 22)
test 3: AAST versus GBM	291 × 200	203 × 200 (GBM = 183, AAST = 20)	88 × 200 (GBM = 78, AAST = 10)

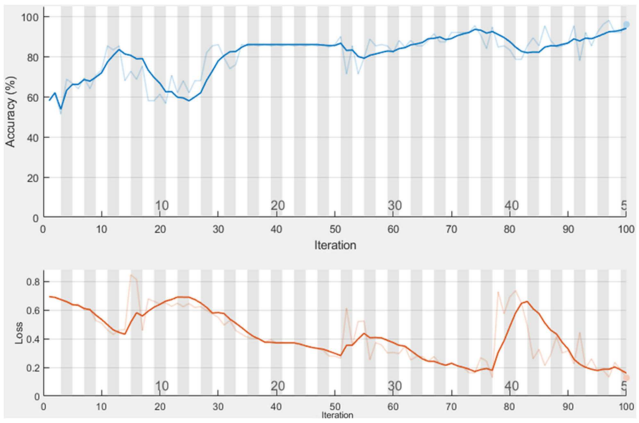

Fig. 12 *Testing performance and loss function fluctuation with GBM versus MEN for test 1*

In the study, PAST, which is one of the brain tumours used in the study for grading of brain tumours, is a GI benign brain tumours. On the other hand, DAST is a GII tumour and has a slightly abnormal appearance. However, they are often considered as benign. AAST is a malignant GIII tumour. GBM tumour cells used in the study are GIV malignant tumours and, where a large portion of the tumour cells reproduce and divide rapidly. GBMs are generally found in the cerebral hemispheres of the brain but can also be found in different parts of the brain. GBMs represent about 15% of all primary brain tumours. GBMs are slightly more common in men than in women and the possibility of these tumours increases with age [65]. MEN are benign tumours that usually arise from the brain and spinal cord sheaths. Although they are mostly seen as slow-growing and GI tumours according to the WHO classification, they are rarely seen as malignant GII and GIII.

Firstly, a vector of 1×200 dimensions using MRS signals was specified for each patient's data. The *X*-axis of the MRS signal represents data of the MRS process implemented for the brain tissue. Then, data of all patients were summed in a single matrix. As a result, the sub-set with a matrix of 144×200 was created for GI and GIV brain tumour grading in the MEN versus GBM test (test 1). The sub-set with a 112×200 matrix was created in the PAST + DAST versus GBM test for GI + GII and GIV brain tumour grading (test 2), and the sub-set with 97×200 matrix was created in the AAST versus GBM test for GIII and GIV brain tumour grading (test 3). However, due to the limited data available in the MRS dataset, the sub-sets were increased three times since more data was needed for training LSTM networks. In the last stage, matrices with 432×200, 336×200, and 291×200 dimensions were obtained for experimental studies. In addition, label vectors of 432×1, 336×1, 291×1 dimensions were also determined for the type of brain tumour of the patient in each row. In order to obtain higher ACC in the classification process, the dataset is split into a training set (70%) and a test set (30%) for the use of classification. The distribution of training and test sets is presented in Table 4.

In addition, ACC, SEN, and specificity (SPE) parametric measurement criteria were used to measure the performance of the tests. Equations for ACC, SEN, and SPE are given in (6)–(8), respectively, where TP = true positive, TN = true negative, FN = false negative and FP = false positive

$$\text{ACC}: \frac{\text{TP} + \text{TN}}{\text{TP} + \text{TN} + \text{FN} + \text{FP}} \tag{6}$$

$$\text{SEN}: \frac{\text{TP}}{\text{TP} + \text{FN}} \tag{7}$$

$$\text{SPE}: \frac{\text{TN}}{\text{TN} + \text{FP}} \tag{8}$$

In the proposed LSTM-based system for experimental tests, the MRS signal values and label values of each patient were matched and the data was split into mini-batches. Then, the data of the patients were randomly divided as training and test data according to the rates. After the dataset was distributed to the training and testing sets, the LSTM layer was specified. In the first layer, the input sequence was specified as one dimensional. Then, the training and testing process was performed over this data and designed the LSTM layer. Since the obtained first results were achieved with an average ACC between 60 and 70%, the data were re-trained with feature extraction before putting the data into training. In addition, the input sequence of the LSTM network was re-arranged as two dimensional. After these changes, the data were re-trained. As a result of training and testing conducted using the feature extraction process, the performance rates of the system increased significantly. Moreover, the input sequence of the system, which was designed as one-dimensional in the first LSTM model, was updated as two-dimensional and the system was re-trained accordingly.

In the experiment, the grade classification process of brain tumours was performed between GBM (GIV) and MEN (GI) for test 1, which was the first testing for the grading of brain tumours. As a result of training, 98.0% ACC performance was achieved for test set within test 1 as seen in Fig. 12.

The confusion matrix obtained in test 1 (MEN versus GBM) comparison is presented in Table 5 for experimental studies. As can be seen from this table, three MRS data in the MEN class were incorrectly classified as GBM. In total, 127 of the 130 MRS data were classified successfully and MEN and GBM type brain tumours were distinguished with 98.0% ACC rate. In addition, we achieved 100.0% SEN and 96.3% SPE rates for test 1.

Within test 2, the ACC and loss values of the LSTM network are shown in Fig. 13 for PAST (GI) + DAST (GII) and GBM (GIV) classification. In addition, performance results obtained in test 2 are denoted in Table 6 for experimental studies. As seen in the confusion matrix, in total 100 MRS data were successfully classified and grading of PAST + DAST and GBM brain tumours was achieved with high results of 100.0% for all ACC, SEN, and SPE.

The performance results of the LSTM network for test 3 are shown in Fig. 14 for GBM (GIV) and AAST (GIII) within grade

Table 5 Grading test performance results for MEN versus GBM tumour types

Test 1	Prediction		Total	Results, %
MEN (GI) versus GBM (GIV)	MEN	GBM		
actual				
MEN	49 (TP)	3 (FN)	52	ACC: 98.0; SEN: 100.0; SPE: 96.3
GBM	0 (FP)	78 (TN)	78	
total	49	81	130	

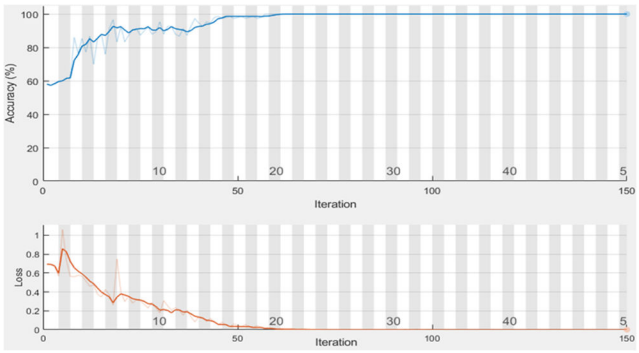

Fig. 13 *Testing performance with GBM versus PAST + DAST for test 2 within grade classification*

Table 6 Test performance results for PAST + DAST versus GBM tumour types

Test 2	Prediction		Total	Results, %
PAST + DAST (GI + GII) versus GBM (GIV)	PAST + DAST	GBM		
actual				
PAST + DAST	22 (TP)	0 (FN)	22	ACC: 100.0; SEN: 100.0; SPE:100.0
GBM	0 (FP)	78 (TN)	78	
total	22	78	100	

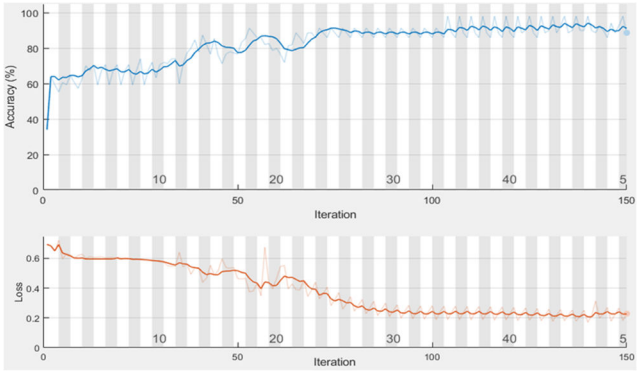

Fig. 14 *Testing performance and loss function with GBM versus AAST for test 3*

classification. In addition, the confusion matrix relating to these obtained results is presented in Table 7 for performance results. We can see in this table, three MRS data in the AAST class were incorrectly classified as GBM. In total, 85 of the 88 MRS data were successfully classified and the grading of MEN and GBM type brain tumours was achieved with a high result of 96.6% ACC. Moreover, we obtained 100.0% SEN and 96.3% SPE rates for test 3.

7 Discussion

In summary for experimental tests, when the results obtained in test 1, test 2, and test 3 procedures performed on the proposed LSTM network for grading brain tumours on MRS data were examined, the performance rates of the system were found to be significantly higher. As a result of three different test procedures, grading of brain tumours was acceptable with an average of 98.20% ACC, 100% SEN, and 97.53% SPE performance rates. Therefore, it was seen that brain tumours were successfully graded using LSTM networks on MRS data. In addition, it was obtained that the MRS data classified incorrectly in test 1 and test 3 belonged to one patient. The data was increased three times in the pre-processing grade in order to train the LSTM network to give better results. As a result, the incorrect data occurred three times in the test process.

Some studies have been proposed for grading brain tumours using both MRI images and MRS data. However, it is very difficult to compare these studies in terms of performance because most of these studies have different datasets and various methodologies. Nevertheless, as in Table 8, a comparison of some studies on the grading of brain tumours is summarised. This summary table shows that the method proposed in this study using LSTM networks on MRS data is successful in grading brain tumours when comparing other studies. Moreover, in the grading of brain tumours using the proposed LSTM-based model, the average area under the curve (AUC) value of the receiver operating characteristic (ROC) curve is measured with high performance of 0.9936 for three grade classification tests and ROC curve graphic and AUC values of the tests are denoted in Fig. 15.

Table 7 Test performance results for AAST versus GBM tumour types

Test 3	Prediction		Total	Results, %
AAST (GIII) versus GBM (GIV)	AAST	GBM		
actual				
AAST	7 (TP)	3 (FN)	10	ACC: 96.6; SEN: 100.0; SPE: 96.3
GBM	0 (FP)	78 (FP)	78	
total	7	81	88	

Table 8 Comparison of the proposed method with other reported studies

The study	Dataset	Data type	Method	ACC	SEN	SPE	AUC
Chen *et al.* [45]	their own dataset	MRS	PCA and SIMCA	87.00	87.00	93.00	NA
Wang *et al.* [47]	their own dataset	MRS	LS-SVM with radial basis functions (RBF)	87.7	NA	NA	NA
Tate *et al.* [18]	INTERPRET [44]	MRS	DSS [66]	89.00	NA	NA	NA
Julia-Sape *et al.* [46]	INTERPRET [44]	MRS	DSS [66]	NA	NA	NA	0.93
Anaraki *et al.* [48]	TCGA, REMBRANDT, The Cancer Imaging Archive (TCIA), IXI, and their own dataset	MRI	CNN and GA	94.2	NA	NA	NA
Sajjad *et al.* [49]	radiopaedia, brain tumour dataset [50]	MRI	CNN	94.58	96.12	88.41	NA
proposed study	INTERPRET [44]	MRS	LSTM	98.20	100.00	97.53	0.9936

NA: not applicable.

8 Conclusions

In this study, an automated computer-assisted system for classification brain tumours grade proposed is based on LSTM neural networks using MRS data. The proposed method was achieved brain tumour grading with high precision. Firstly, a dataset was prepared on MRS signals from the INTERPRET project database. Then, MRS signals of brain tumour with different grades were classified using the LSTM network without feature extraction. In this step, the success rate of the training phase varied between 60 and 70% with ACC. In the next step, additional features from MRS signals such as instantaneous frequency and spectral entropy were extracted according to spectrogram data. Afterwards, spectrograms showing the energy distributions of each MRS signal type were obtained to decide which features to extract. In addition, training and test data were increased three times using data augmentation in order to make the training process more efficient. In the experimental studies, the frequency of the MRS signals for the tests was determined as 64 and dataset split into 70% training and 30% test set. Therefore, the classification performance of the system was increased by the feature extraction from MRS signals in order to help improve the training and test ACC of the LSTM classifier. Finally, the experimental results were obtained in test 1, test 2 and test 3 procedures performed on the proposed LSTM network for grading brain tumours on MRS data. As a result of three tests, grading of brain tumours was classified with an average of 98.20% ACC, 100% SEN, and 97.53% SPE performance rates, respectively. The performance rates of the system were achieved to be significantly acceptable. In addition, the proposed method can be used as a secondary tool for grading of brain tumours as a non-invasive procedure.

Although brain tumours were successfully graded on MRS data using LSTM networks, it was obtained that the MRS data classified incorrectly in test 1 and test 3 belonged to one patient. Since the data was increased three times in the pre-processing step in order to train the LSTM network to give better results, the incorrect data occurred three times in the test process. It is thought that the classification of these data incorrectly was due to the fact that the MRS values were close and that the available values were sufficient to train the network, but not enough for testing.

In the future works, it is planned to conduct experimental studies on different types of brain tumours at different grades on more MRS data and to compare the results with various deep leaning models. Even though the proposed method gains better performance compared to some similar literature works, larger datasets, other deep learning methods, and different pre-trained network models may achieve better classification performances.

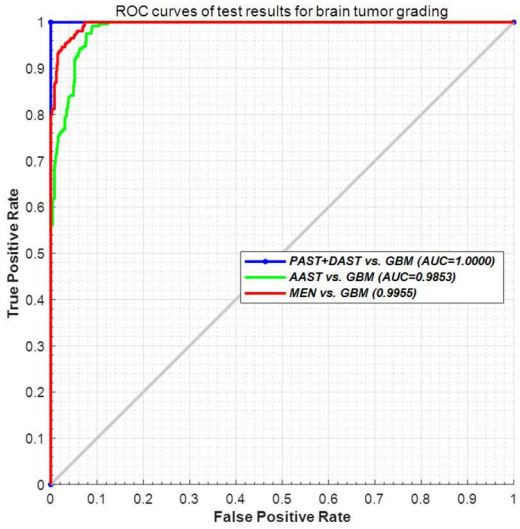

Fig. 15 *ROC curves and AUC values for the proposed method*

9 Acknowledgments

The authors thank the entire project team, especially Dr Margarida Julià-Sapé, for allowing the use of data from the MRS database created within the INTERPRET project.

10 References

[1] Causes of death. Available at https://ourworldindata.org/causes-of-death, accessed 27 October 2019

[2] Cancer today: data visualization tools for exploring the global cancer burden in 2018. Available at http://gco.iarc.fr/today/home, accessed 27 October 2019

[3] Amin, J., Sharif, M., Yasmin, M., *et al.*: 'A distinctive approach in brain tumor detection and classification using MRI', *Pattern Recognit. Lett.*, 2017, to appear

[4] Louis, D.N., Perry, A., Reifenberger, G., *et al.*: 'The 2016 world health organization classification of tumors of the central nervous system: a summary', *Acta Neuropathol.*, 2016, **131**, (6), pp. 803–820

[5] Bray, F., Ferlay, J., Soerjomataram, I., *et al.*: 'Global cancer statistics 2018: Globocan estimates of incidence and mortality worldwide for 36 cancers in 185 countries', *CA-Cancer J. Clin.*, 2018, **68**, (6), pp. 394–424

[6] Logeswari, T., Karnan, M.: 'An improved implementation of brain tumor detection using segmentation based on hierarchical self organizing map', *Int. J. Comput. Theor. Eng.*, 2010, **2**, (4), p. 591

[7] El-Dahshan, E.-S.A., Mohsen, H.M., Revett, K., *et al.*: 'Computer-aided diagnosis of human brain tumor through MRI: a survey and a new algorithm', *Expert Syst Appl*, 2014, **41**, (11), pp. 5526–5545

[8] Georgiadis, P., Cavouras, D., Kalatzis, I., *et al.*: 'Improving brain tumor characterization on MRI by probabilistic neural networks and non-linear

transformation of textural features', *Comput. Methods Programs Biomed.*, 2008, **89**, (1), pp. 24–32
[9] Kondziolka, D., Lunsford, L.D., Martinez, A.J.: 'Unreliability of contemporary neurodiagnostic imaging in evaluating suspected adult supratentorial (low-grade) astrocytoma', *J. Neurosurg.*, 1993, **79**, (4), pp. 533–536
[10] Bernstein, M., Parrent, A.G.: 'Complications of CT-guided stereotactic biopsy of intra-axial brain lesions', *J. Neurosurg.*, 1994, **81**, (2), pp. 165–168
[11] Zeng, Q., Liu, H., Zhang, K., *et al.*: 'Noninvasive evaluation of cerebral glioma grade by using multivoxel 3D proton MR spectroscopy', *Magn. Reson. Imaging*, 2011, **29**, (1), pp. 25–31
[12] Möller-Hartmann, W., Herminghaus, S., Krings, T., *et al.*: 'Clinical application of proton magnetic resonance spectroscopy in the diagnosis of intracranial mass lesions', *Neuroradiology*, 2002, **44**, (5), pp. 371–381
[13] Bulik, M., Jancalek, R., Vanicek, J., *et al.*: 'Potential of MR spectroscopy for assessment of glioma grading', *Clin. Neurol. Neurosurg.*, 2013, **115**, (2), pp. 146–153
[14] Yüksel, C., Öngür, D.: 'Magnetic resonance spectroscopy studies of glutamate-related abnormalities in mood disorders', *Biol. Psychiatry*, 2010, **68**, (9), pp. 785–794
[15] O'Donnell-Luria, A.H., Lin, A.P., Merugumala, S.K., *et al.*: 'Brain MRS glutamine as a biomarker to guide therapy of hyperammonemic coma', *Mol. Genet. Metab.*, 2017, **121**, (1), pp. 9–15
[16] Hagberg, G.: 'From magnetic resonance spectroscopy to classification of tumors. A review of pattern recognition methods', *NMR Biomed.*, 1998, **11**, (4–5), pp. 148–156
[17] Tate, A.R., Majós, C., Moreno, A., *et al.*: 'Automated classification of short echo time in in vivo ^{1}H brain tumor spectra: a multicenter study', *Magn. Reson. Med.*, 2003, **49**, (1), pp. 29–36
[18] Tate, A.R., Underwood, J., Acosta, D.M., *et al.*: 'Development of a decision support system for diagnosis and grading of brain tumours using in vivo magnetic resonance single voxel spectra', *NMR Biomed.*, 2006, **19**, (4), pp. 411–434
[19] González-Vélez, H., Mier, M., Julià-Sapé, M., *et al.*: 'HealthAgents: distributed multi-agent brain tumor diagnosis and prognosis', *Appl. Intell.*, 2009, **30**, (3), pp. 191–202
[20] Devos, A., Lukas, L., Suykens, J., *et al.*: 'Classification of brain tumours using short echo time ^{1}H MR Spectra', *J. Magn. Reson.*, 2004, **170**, (1), pp. 164–175
[21] Howe, F.A., Opstad, K.S.: '1 h MR spectroscopy of brain tumours and masses', *NMR Biomed.*, 2003, **16**, (3), pp. 123–131
[22] Arizmendi, C., Sierra, D.A., Vellido, A., *et al.*: 'Automated classification of brain tumours from short echo time in vivo MRS data using Gaussian decomposition and Bayesian neural networks', *Expert Syst. Appl.*, 2014, **41**, (11), pp. 5296–5307
[23] Dimou, I., Tsougos, I., Tsolaki, E., *et al.*: 'Brain lesion classification using 3t MRS spectra and paired SVM kernels', *Biomed. Signal Proc. Control*, 2011, **6**, (3), pp. 314–320
[24] Vicente, J., Fuster-Garcia, E., Tortajada, S., *et al.*: 'Accurate classification of childhood brain tumours by in vivo ^{1}H MRS – a multi-centre study', *Eur. J. Cancer*, 2013, **49**, (3), pp. 658–667
[25] Goebell, E., Paustenbach, S., Vaeterlein, O., *et al.*: 'Low-grade and anaplastic gliomas: differences in architecture evaluated with diffusion-tensor MR imaging', *Radiology*, 2006, **239**, (1), pp. 217–222
[26] Server, A., Kulle, B., Gadmar, Ø.B., *et al.*: 'Measurements of diagnostic examination performance using quantitative apparent diffusion coefficient and proton MR spectroscopic imaging in the preoperative evaluation of tumor grade in cerebral gliomas', *Eur. J. Radiol.*, 2011, **80**, (2), pp. 462–470
[27] Stadlbauer, A., Gruber, S., Nimsky, C., *et al.*: 'Preoperative grading of gliomas by using metabolite quantification with high-spatial-resolution proton MR spectroscopic imaging', *Radiology*, 2006, **238**, (3), pp. 958–969
[28] Zonari, P., Baraldi, P., Crisi, G.: 'Multimodal MRI in the characterization of glial neoplasms: the combined role of single-voxel MR spectroscopy, diffusion imaging and echo-planar perfusion imaging', *Neuroradiology*, 2007, **49**, (10), pp. 795–803
[29] Nelson, S.J., Graves, E., Pirzkall, A., *et al.*: 'In vivo molecular imaging for planning radiation therapy of gliomas: an application of ^{1}H MRSI', *J. Magn. Reson. Imag.*, 2002, **16**, (4), pp. 464–476
[30] Dowling, C., Bollen, A.W., Noworolski, S.M., *et al.*: 'Preoperative proton MR spectroscopic imaging of brain tumors: correlation with histopathologic analysis of resection specimens', *Am. J. Neuroradiol.*, 2001, **22**, (4), pp. 604–612
[31] Liu, H., Hall, W.A., Martin, A.J., *et al.*: 'MR-guided and MR-monitored neurosurgical procedures at 1.5 T', *J. Comput. Assist. Tomogr.*, 2000, **24**, (6), pp. 909–918
[32] Dimou, I., Tsougos, I., Tsolaki, E., *et al.*: 'Classification of pathological human brain lesions using magnetic resonance spectroscopy at 3T'. World Congress on Medical Physics and Biomedical Engineering, 7–12 September 2009, Munich, Germany, 2009, pp. 1368–1370
[33] Majos, C., Aguilera, C., Alonso, J., *et al.*: 'Proton MR spectroscopy improves discrimination between tumor and pseudotumoral lesion in solid brain masses', *Am. J. Neuroradiol.*, 2009, **30**, (3), pp. 544–551
[34] Weis, J., Ring, P., Olofsson, T., *et al.*: 'Short echo time MR spectroscopy of brain tumors: grading of cerebral gliomas by correlation analysis of normalized spectral amplitudes', *J. Magn. Reson. Imag.*, 2010, **31**, (1), pp. 39–45
[35] Luts, J., Heerschap, A., Suykens, J.A., *et al.*: 'A combined MRI and MRSI based multiclass system for brain tumour recognition using LS-SVMs with class probabilities and feature selection', *Artif. Intell. Med.*, 2007, **40**, (2), pp. 87–102
[36] Meyerand, M.E., Pipas, J.M., Mamourian, A., *et al.*: 'Classification of biopsy-confirmed brain tumors using single-voxel MR spectroscopy', *Am. J. Neuroradiol.*, 1999, **20**, (1), pp. 117–123
[37] Law, M., Yang, S., Wang, H., *et al.*: 'Glioma grading: sensitivity, specificity, and predictive values of perfusion MR imaging and proton MR spectroscopic imaging compared with conventional MR imaging', *Am. J. Neuroradiol.*, 2003, **24**, (10), pp. 1989–1998
[38] Ishimaru, H., Morikawa, M., Iwanaga, S., *et al.*: 'Differentiation between high-grade glioma and metastatic brain tumor using single-voxel proton MR spectroscopy', *Eur. Radiol.*, 2001, **11**, (9), pp. 1784–1791
[39] Arizmendi, C., Vellido, A., Romero, E.: 'Classification of human brain tumours from MRS data using discrete wavelet transform and Bayesian neural networks', *Expert Syst. Appl.*, 2012, **39**, (5), pp. 5223–5232
[40] Naser, R.K.A., Hassan, A.A.K., Shabana, A.M., *et al.*: 'Role of magnetic resonance spectroscopy in grading of primary brain tumors', *Egypt. J. Radiol. Nucl. Med.*, 2016, **47**, (2), pp. 577–584
[41] Manias, K., Gill, S.K., Zarinabad, N., *et al.*: 'Evaluation of the added value of ^{1}H-magnetic resonance spectroscopy for the diagnosis of pediatric brain lesions in clinical practice', *Neurooncol. Pract.*, 2017, **5**, (1), pp. 18–27
[42] Zou, Q.-G., Xu, H.-B., Liu, F., *et al.*: 'In the assessment of supratentorial glioma grade: the combined role of multivoxel proton MR spectroscopy and diffusion tensor imaging', *Clin. Radiol.*, 2011, **66**, (10), pp. 953–960
[43] Afshar, P., Mohammadi, A., Plataniotis, K.N.: 'Brain tumor type classification via capsule networks'. 2018 25th IEEE Int. Conf. on Image Processing (ICIP), Athens, Greece, 2018, pp. 3129–3133
[44] 'International network for pattern recognition of tumours using magnetic resonance', Available at http://gabrmn.uab.es/interpret/, accessed 27 October 2019
[45] Chen, W., Lou, H., Zhang, H., *et al.*: 'Grade classification of neuroepithelial tumors using high-resolution magic-angle spinning proton nuclear magnetic resonance spectroscopy and pattern recognition', *Sci. Chin. Life Sci.*, 2011, **54**, (7), pp. 606–616
[46] Julià-Sapé, M., Coronel, I., Majós, C., *et al.*: 'Prospective diagnostic performance evaluation of single-voxel ^{1}H MRS for typing and grading of brain tumours', *NMR Biomed.*, 2012, **25**, (4), pp. 661–673
[47] Wang, L., Wan, S., Sun, Y., *et al.*: 'Automatic classification of brain tumor by in vivo MRS data based on LDA and SVM'. Seventh Int. Conf. on Measuring Technology and Mechatronics Automation, Nanchang, China, 2015, pp. 213–216
[48] Anaraki, A.K., Ayati, M., Kazemi, F.: 'Magnetic resonance imaging-based brain tumor grades classification and grading via convolutional neural networks and genetic algorithms', *Biocybern. Biomed. Eng.*, 2019, **39**, (1), pp. 63–74
[49] Sajjad, M., Khan, S., Muhammad, K., *et al.*: 'Multi-grade brain tumor classification using deep CNN with extensive data augmentation', *J. Comput. Sci.*, 2019, **30**, pp. 174–182
[50] Cheng, J., Huang, W., Cao, S., *et al.*: 'Enhanced performance of brain tumor classification via tumor region augmentation and partition', *PLOS One*, 2015, **10**, (10), p. e0140381
[51] Skoch, A., Jiru, F., Bunke, J.: 'Spectroscopic imaging: basic principles', *Eur. J. Radiol.*, 2008, **67**, (2), pp. 230–239
[52] Hajek, M., Dezortova, M.: 'Introduction to clinical in vivo MR spectroscopy', *Eur. J. Radiol.*, 2008, **67**, (2), pp. 185–193
[53] Kwock, L.: 'Localized MR spectroscopy: basic principles', *Neuroimaging Clin. N. Am.*, 1998, **8**, (4), pp. 713–731
[54] Callot, V., Galanaud, D., Le Fur, Y., *et al.*: '^{1}H MR spectroscopy of human brain tumours: a practical approach', *Clin. Imag.*, 2008, **67**, (2), pp. 268–274
[55] Tian, Y., Zhang, K., Li, J., *et al.*: 'LSTM-based traffic flow prediction with missing data', *Neurocomputing*, 2018, **318**, pp. 297–305
[56] Yu, R., Gao, J., Yu, M., *et al.*: 'LSTM-EFG for wind power forecasting based on sequential correlation features', *Future Gener. Comput. Syst.*, 2019, **93**, pp. 33–42
[57] Cao, J., Li, Z., Li, J.: 'Financial time series forecasting model based on CEEMDAN and LSTM', *Physica A*, 2019, **519**, pp. 127–139
[58] Jian, C., Yang, M., Zhang, M.: 'Mobile terminal trajectory recognition based on improved LSTM model', *IET Image Process.*, 2019, **13**, (11), pp. 1914–1921
[59] Li, X., Yu, C., Su, F., *et al.*: 'Novel training algorithms for long short-term memory neural network', *IET Signal Process.*, 2018, **13**, (3), pp. 304–308
[60] Graves, A.: 'Generating sequences with recurrent neural networks', arXiv preprint arXiv:1308.0850, 2013
[61] Salehinejad, H., Sankar, S., Barfett, J., *et al.*: 'Recent advances in recurrent neural networks', arXiv preprint arXiv:1801.01078, 2017
[62] Karpathy, A., Johnson, J., Fei-Fei, L.: 'Visualizing and understanding recurrent networks', arXiv preprint arXiv:1506.02078, 2015
[63] Wu, C.-Y., Ahmed, A., Beutel, A., *et al.*: 'Recurrent recommender networks'. The Tenth ACM int. Conf. on Web Search and Data Mining, Cambridge, UK, 2017, pp. 495–503
[64] Misra, H., Ikbal, S., Bourlard, H., *et al.*: 'Spectral entropy based feature for robust ASR'. IEEE Int. Conf. on Acoustics, Speech, and Signal Processing, Montreal, Quebec, Canada, 2004, p. I-193
[65] Abta. Available at https://www.abta.org/wp-content/uploads/2018/03/newly-diagnosed-1.pdf, accessed 27 October 2019
[66] Grup d'aplicacions biomèdiques De La ressonància magnètica nuclear (GABRMN) interpret DSS. Available at http://gabrmn.uab.es/dss, accessed 27 October 2019